RSC Advances

PAPER

View Article Online
View Journal | View Issue

Cite this: *RSC Adv.*, 2023, **13**, 6002

Low-cost diatomite supported binary transition metal sulfates: an efficient reusable solid catalyst for biodiesel synthesis†

Weiqing Chen,[a] Zhaoji Wu,[a] Ruoxue Peng,[a] Wenjuan Wu,[a] Xiaonan Li,[a] Dan Cao,[a] Zhigang Zhang*[ab] and Kui Niu*[ab]

Using a simple method of impregnation and then calcination, diatomite supported binary transition metal sulfates (Fe and Zr, designated as $Fe_2(SO_4)_3$&$Zr(SO_4)_2$@diatomite) were prepared and used as a catalyst in the preparation of renewable biofuels. The synthesised $Fe_2(SO_4)_3$&$Zr(SO_4)_2$@diatomite catalyst ($Fe_2(SO_4)_3$: $Zr(SO_4)_2$: diatomite = 1 : 2 : 6, mass ratio) was thoroughly characterised using transmission electron microscopy (TEM), X-ray diffraction (XRD), Fourier-transform infrared (FTIR) spectroscopy, microbeam X-ray fluorescence (μ-XRF) spectroscopy and thermogravimetric analysis (TG). The results demonstrated that the sulfate was successfully loaded onto the diatomite with a uniform distribution. The N_2 adsorption/desorption analysis indicated that the catalyst's specific surface area was 1.54 $m^2\ g^{-1}$. The catalyst exhibited outstanding performance in the preparation of renewable biofuel (biodiesel) from waste fatty acids and the optimal parameters were methanol-to-oil 1.25 : 1, reaction temperature 70 °C, catalyst concentration 10 wt%, reaction time 4 h. The conversion was found to reach 98.90% under optimal parameters, which is better than that of $Fe_2(SO_4)_3 \cdot xH_2O$, $Zr(SO_4)_2 \cdot 4H_2O$, $Fe_2(SO_4)_3$@diatomite and $Zr(SO_4)_2$@diatomite. Moreover, the catalyst can be recycled by simple filtration and reused for three cycles after regeneration without noticeable reduction in catalytic activity.

Received 13th December 2022
Accepted 5th February 2023

DOI: 10.1039/d2ra07947j

rsc.li/rsc-advances

1 Introduction

With increasing energy demand, the consumption of fossil fuels, and their negative impact on the environment, such as environmental pollution, global warming, and rising sea levels, great attention has been given to researching renewable and clean biofuels.[1–4] Biodiesel, a green, biodegradable, renewable and sustainable biofuel, is usually made from waste vegetable oils and animal fats. The composition of biodiesel is alkyl esters of fatty acids derived from vegetable oils and fats. Compared with traditional fuels, it has many advantages, such as it is nontoxic, biodegradable, has a low amount of sulfur, has a high energy density, excellent combustion performance, less particulate pollutants, less greenhouse gases (mainly CO_2 emissions) and carbon monoxide emissions, it is safer to handle, and so on.[5–7] In particular, biodiesel can be applied directly in diesel engines or blended with fossil fuel diesel in any proportion.[8] Hence, a lot of researchers are investigating biodiesel because from a strategic standpoint it is one of the most significant fossil fuel alternatives.

Biodiesel is usually made from animal and vegetable oils using the chemical processes of esterification and transesterification with methanol or ethanol in the presence of a catalyst.[9] In production processes, catalysts always play a central role and affect the biodiesel yield and the long-term viability of the industrial process.[10,11] They are often classified into homogeneous catalysts or heterogeneous catalysts.[12–14] Homogeneous catalysts, such as sulfuric acid (H_2SO_4), H_3PO_4, KOH, and potassium hydroxide (NaOH), have many disadvantages, such as the difficulty of separation, and inability to be reused, generation of wastewater and corrosion of the reactor.[15–17] Heterogeneous catalysts, including heterogeneous acids and bases, are considered as a potential alternative because of their easy separation from the reaction mixture, good stability, excellent reactivity and easy recovery.[16,18–21]

However, waste vegetable oils and fats usually contain high levels of fatty acids due to them becoming rancid during collection and processing. When employing base catalysts, these fatty acids cannot be transformed into fatty acid alkyl esters (biodiesel) by esterification, resulting in low yields. Therefore, heterogeneous acids are considered appropriate for the catalysis of biodiesel manufacture from waste vegetable oils and fats, because they can stimulate esterification of the fatty acids and transesterification of the triglycerides into alkyl esters

[a]*College of Chemical Engineering, Hebei Normal University of Science & Technology, Qinhuangdao, China 066600. E-mail: zgzhang333@163.com*

[b]*Hebei Key Laboratory of Active Components and Functions in Natural Products, Qinhuangdao, China 066600. E-mail: niukui007@163.com*

† Electronic supplementary information (ESI) available. See DOI: https://doi.org/10.1039/d2ra07947j

simultaneously. Many types of heterogeneous acids, including solid superacid (especially sulfated metal oxide),[22–25] cation exchange resin,[26–28] supported heteropoly acid,[29–31] sulfonated carbon-based solid acids[32–34] and so on, have been widely studied by researchers during the past decade. However, few of them have been widely used in industrial production for various factors such as high cost, complexity and the generation of pollutants during preparation. For industrial biodiesel manufacture using waste vegetable oils and fats, it is crucial to design heterogeneous acidic catalysts with high efficiency, stability, acceptable reusability, low cost and environmental benefits.

Transition metal sulfates such as ferric sulfate ($Fe_2(SO_4)_3$) and zirconium sulfate ($Zr(SO_4)_2$), as solid Lewis acids, exhibited excellent catalytic performance in the catalysis of esterification.[35–38] Compared with $Zr(SO_4)_2$, $Fe_2(SO_4)_3$ is inexpensive and readily available, but it is susceptible to moisture absorption which affects its catalytic performance in the esterification reaction. In addition, although $Fe_2(SO_4)_3$ and $Zr(SO_4)_2$ are insoluble in oil, they can be slightly soluble in methanol and will dissolve in the water formed during esterification, which will lead to loss of the catalyst and inferior reusability.[35] To address these problems, immobilising them on suitable carrier was a good strategy to avoid the dissolution, and loss of the catalytic active substance, greatly improving their catalytic activity and stability.

Diatomite is a typical natural siliceous rock mainly composed of amorphous silica with excellent properties, such as low cost, porosity, chemical inertness, compatibility and availability for surface modification.[39,40] Hence, diatomite has been considered as a promising support/template and used for broad range of applications including energy conversion and storage,[41–44] water remediation,[45–48] and drug delivery.[49–51] Furthermore, diatomite has also been used as a desirable catalyst support in many organic chemical reactions.[52,53] Some diatomite supported basic heterogeneous compounds, such as diatomite supported CaO/MgO and diatomite-supported KOH, have been developed for biodiesel preparation.[54–56]

In addition, the cost of diatomite is usually much lower than that of other supports such as zeolite,[57,58] alumina,[59,60] activated carbon[61,62] and so on. The price of diatomite reported online is about RMB 2200 per ton, whereas activated carbon is usually RMB 4500–16 000 per ton, alumina is about RMB 7200 per ton, and zeolite is about RMB 9000 per ton.[63,64] Consequently, immobilising $Fe_2(SO_4)_3$ and $Zr(SO_4)_2$ on diatomite may be a good strategy. In this study, the $Fe_2(SO_4)_3$&$Zr(SO_4)_2$@-diatomite catalyst was prepared using simple impregnation and calcination (Scheme 1). The method for the synthesis of this novel catalyst is not only simple but also economical, which is beneficial for industrial applications.

2 Materials and methods

2.1 Materials

Ferric sulfate hydrate ($Fe_2(SO_4)_3 \cdot xH_2O$, Fe content 21–23 wt%), zirconium sulfate tetrahydrate ($Zr(SO_4)_2 \cdot 4H_2O$, AR), methanol (99.5% purity), and diatomite (median diameter: 19.6 μm) were purchased from Shanghai Aladdin Bio-Chem Technology (Shanghai, China). The H_2SO_4 (98% purity) and potassium hydroxide (KOH, ≥85% purity) were purchased from Institute of Tianjin Chemical Reagent Research Institute (Tianjin, China). Waste animal and vegetable oils (moisture content 2.28 wt%, ash content 0.52 wt%) were collected from a municipal sewer. Waste fatty acids (acid value 195.50 mg KOH per g, saponification value 205.82 mg KOH per g) were extracted from waste animal and vegetable oils. The composition of the waste fatty acids was: palmitic acid (C16:0) 22.99 wt%, stearic acid (C18:0) 5.62 wt%, oleic acid (C18:1) 36.68 wt%, linoleic acid (C18:2) 26.19 wt%, and dietary linolenic acid (C18:3) 2.86 wt%.

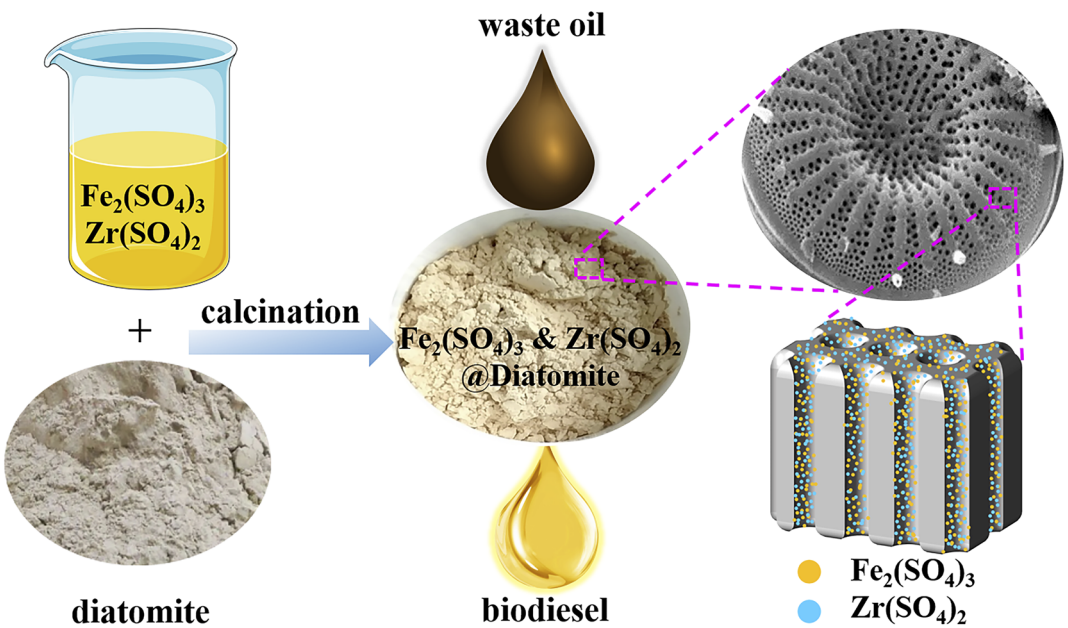

Scheme 1 The preparation of $Fe_2(SO_4)_3$ and $Zr(SO_4)_2$@diatomite.

2.2 Methods

2.2.1 Modification of diatomite. In order to obtain a perfect porous structure, diatomite modification was performed by treating it with H_2SO_4. Firstly, 100 g of diatomite was immersed in 300 mL of an aqueous solution of H_2SO_4 (3 mol L^{-1}) which was then stirred at room temperature for 4 h. Afterwards, the mixture was filtered at reduced pressure, and the obtained filter cake was thoroughly washed with deionised water until the pH value of the filtrate reached 7.0. Next, the filter cake was dried at 110 °C in a drying oven. Finally, the modified diatomite was obtained after calcining at 400 °C for 2 h.

2.2.2 Synthesis of the $Fe_2(SO_4)_3$&$Zr(SO_4)_2$@diatomite catalyst. The $Fe_2(SO_4)_3$&$Zr(SO_4)_2$@diatomite catalyst was prepared by a simple impregnation and calcination process. In brief, 1.33 g of $Fe_2(SO_4)_3 \cdot xH_2O$ and 2.67 g of $Zr(SO_4)_2 \cdot 4H_2O$ were first dissolved in 15 mL of deionised water. Next, 6 g of modified diatomite was impregnated in it and the mixture was agitated at 40 °C for 2 h. After impregnation, it was dried in a drying oven at 110 °C, and then the dried caked matter was ground to powder (median diameter: 19.6 μm) by grinding in a ceramic mortar. Finally, the $Fe_2(SO_4)_3$&$Zr(SO_4)_2$@diatomite catalyst was obtained after calcining at 300 °C for 3 h in a N_2 atmosphere.

2.2.3 Characterisation. The microstructure of the catalyst was observed using TEM (H-7650, Hitachi, Japan) operating at 80.0 kV. The X-ray diffraction was performed using an XRD, (D/Max 2500 PC, Rigaku, Japan) with Cu-Kα radiation and operating conditions of 40 kV, 200 mA, range: 10–80°. Mapping of the chemical composition was carried out using a μ-XRF spectrometer (M4 Tornado, Bruker, Germany). The infrared spectra were measured using an FTIR spectrometer (Tensor 27, Bruker, Germany) with a resolution of 2 cm^{-1} using a KBr tablet as a blank. The N_2 adsorption/desorption isotherms were measured using a volumetric computer-controlled surface analyser (NOVA 2200e, Quantachrome, USA) at 77.3 K (the temperature of liquid N_2). Before measurement, the samples were pre-treated in a tube under vacuum at 300 °C for 4 h to remove any adsorbed substances. A thermogravimetric/differential thermal analyser (STA 409 PC Luxx, Netzsch, Germany) was used for TG analysis, and the measurement was performed at a heating rate of 10 °C min^{-1} under a N_2 flow rate of 50 mL min^{-1}.

2.2.4 Biodiesel preparation. In a typical experiment, a predetermined amount of waste fatty acids (5 g), methanol (2.5 g, 5 g, 6.25 g or 7.5 g) and catalyst (0.2 g, 0.3 g, 0.4 g or 0.5 g) were added into a glass flask (100 mL, three-necked flask, Synthware) equipped with a thermometer, a magnetic stirrer, a reflux condenser and a rubber plug. Then, the reaction was allowed to proceed for a certain time (range from 1 h to 4 h) under the desired temperature (range from 60 °C to 90 °C). The reactor was cooled to room temperature at the end of the reaction. The cooling process takes about 30 minutes. The experiment was performed according to the design of the orthogonal experiment as shown in Table S2 (ESI†). Next, the catalyst was separated by filtration and regenerated by washing with methanol. The extra methanol in the leftover oil was finally eliminated using vacuum rotary evaporation. The conversion of the fatty acids was determined using the following equation:[65,66]

$$\text{Conversion} = \frac{A_0 - A_1}{A_0} \times 100\%$$

where A_0 is the acid value of the waste fatty acids, and A_1 is the acid value of the product.

2.2.5 Determination of acid value. The acid value was determined by titration referring to standard GB/T 5530-2005. The method was as follows: 0.5 g (accurate to 0.0001 g) of waste fatty acids or 1 g (accurate to 0.0001 g) of biodiesel was dissolved in 100 mL of neutralised 95% (v/v) ethanol (v/v), and then the mixture was titrated using an aqueous solution of KOH (0.05 mol L^{-1}) with phenolphthalein as indicator. The acid value was calculated by the following equation:

$$A = \frac{c_{KOH} \times V_{KOH} \times 56.1}{m}$$

where c_{KOH} is the concentration of the KOH solution, V_{KOH} is the volume of the KOH solution consumed during titration, 56.1 is the molecular weight of KOH, and m is the weight of the sample.

3 Results and discussion

3.1 Catalyst characterisation

3.1.1 TEM. The microstructure of the catalyst ($Fe_2(SO_4)_3$ and $Zr(SO_4)_2$@diatomite) was observed using TEM (Fig. 1). As shown in Fig. 1, the diatomite used in this work was porous, and disc like with mesopores. The hierarchical porous surface structure of the diatomite was beneficial to its adsorption ability. Furthermore, it was observed from Fig. 1 that the diatomite still had many pores after loading. This indicated that the pores of the diatomite were not blocked after loading with $Fe_2(SO_4)_3$ and $Zr(SO_4)_2$, and the sulfate was only loaded on the surface of the diatomite and the inner surface of the pores (see Scheme 1). The porous structure of the synthesised catalyst was beneficial to its catalytic efficiency.

3.1.2 XRD. The XRD patterns of the original diatomite, modified diatomite and $Fe_2(SO_4)_3$&$Zr(SO_4)_2$@diatomite catalysts are presented in Fig. 2. As can be seen, the characteristic peaks at 2θ values of 21.6°, 26.5° and 49.9° were associated with

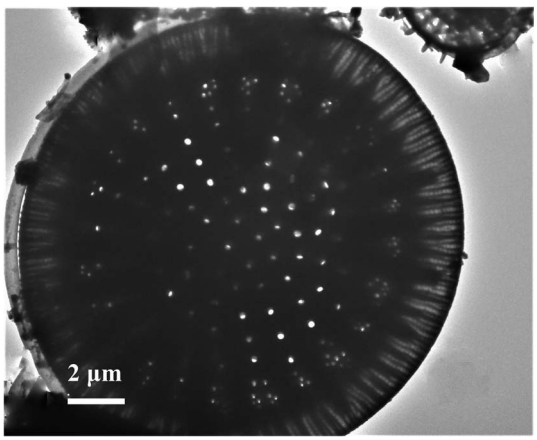

Fig. 1 The TEM image of $Fe_2(SO_4)_3$&$Zr(SO_4)_2$@diatomite.

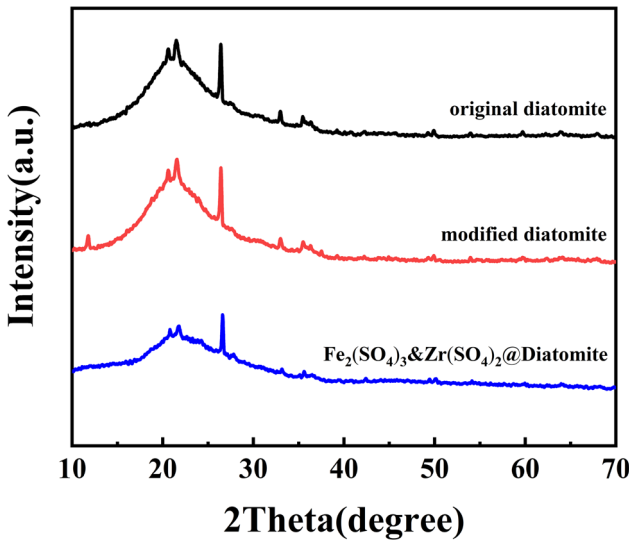

Fig. 2 The XRD patterns of the original diatomite, modified diatomite and $Fe_2(SO_4)_3$&$Zr(SO_4)_2$@diatomite catalyst.

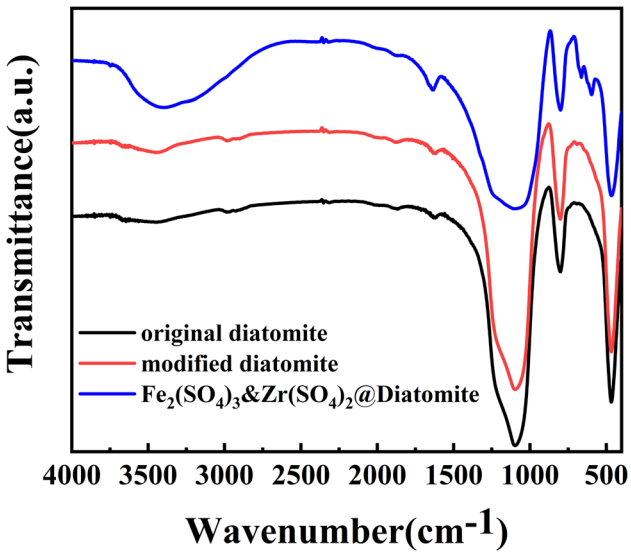

Fig. 4 The FTIR spectra of original diatomite, modified diatomite and the $Fe_2(SO_4)_3$&$Zr(SO_4)_2$@diatomite catalyst.

the crystal planes of the quartz, and the diatomite was amorphous.[67] However, no obvious characteristic peaks of $Zr(SO_4)_2$ appeared after loading. This may be due to the fact that $Zr(SO_4)_2$ was highly dispersed in amorphous form on diatomite, with a loading capacity of 26.7% $Zr(SO_4)_2 \cdot 4H_2O$.[68] Similarly, no obvious characteristic peaks of $Fe_2(SO_4)_3$ appeared either. Hence, $Fe_2(SO_4)_3$ with a loading capacity of 13.3% $Fe_2(SO_4)_3 \cdot xH_2O$ may also be dispersed in an amorphous form on diatomite. These results may show that $Fe_2(SO_4)_3$ and $Zr(SO_4)_2$ were well dispersed in amorphous form on diatomite. The catalytic activity as well as stability of the $Fe_2(SO_4)_3$&$Zr(SO_4)_2$@diatomite catalyst were both improved by the good dispersion.

3.1.3 μ-XRF. To confirm whether the $Fe_2(SO_4)_3$ and $Zr(SO_4)_2$ were loaded onto the diatomite, and the homogeneity of the loading, which was a crucial factor influencing the activity of supported heterogeneous catalysts, the catalyst was characterised using μ-XRF. As shown in Fig. 3, the Fe, S and Zr elements were loaded on diatomite with good dispersity which was identical to that of the original silicon element of diatomite.

3.1.4. FTIR. The FTIR spectra of the original diatomite, modified diatomite and $Fe_2(SO_4)_3$&$Zr(SO_4)_2$@diatomite are shown in Fig. 4. It was observed that both the original diatomite and modified diatomite showed bands at 3396.6 cm^{-1}, 1639.5 cm^{-1}, 1097.5 cm^{-1}, 800.4 cm^{-1} and 468.7 cm^{-1}. The bands at 3396.6 cm^{-1} and 1639.5 cm^{-1} were related to the O–H stretching of water.[69,70] The intense absorption band at about 1097.5 cm^{-1} corresponded to the Si–O–Si asymmetric stretch. The bands centred at 800.4 cm^{-1} and 468.7 cm^{-1} may be due to the Si–O–Si symmetric stretch, and bend vibration, respectively.[71–74] After loading the $Fe_2(SO_4)_3$ and $Zr(SO_4)_2$ onto diatomite, a novel band at 596 cm^{-1} was discovered, that was connected to the stretching of Fe–O in the Fe–O–Si bonds.[75] In addition, the bands at about 1097.5 cm^{-1} became wider, and this revealed the emergence of new Zr–O–Si bonds on the surface of diatomite after the combination of inorganic salt and diatomite.[76,77] These changes strongly confirmed that $Fe_2(SO_4)_3$ and $Zr(SO_4)_2$ were successfully loaded onto the diatomite.

3.1.5 Nitrogen adsorption analysis. The N_2 adsorption/desorption isotherms of modified diatomite and the $Fe_2(SO_4)_3$&$Zr(SO_4)_2$@diatomite catalyst are shown in Fig. 5. Obviously, the modified diatomite and the catalyst had the same form of isotherms, and they all exhibited a type IV sorption behaviour according to the IUPAC classification. In addition, the surface of the modified diatomite was typically mesoporous as indicated by the H_3-type hysteresis loops existing in its isotherm.[78] The specific surface area of the samples decreased from 5.41 $m^2\ g^{-1}$

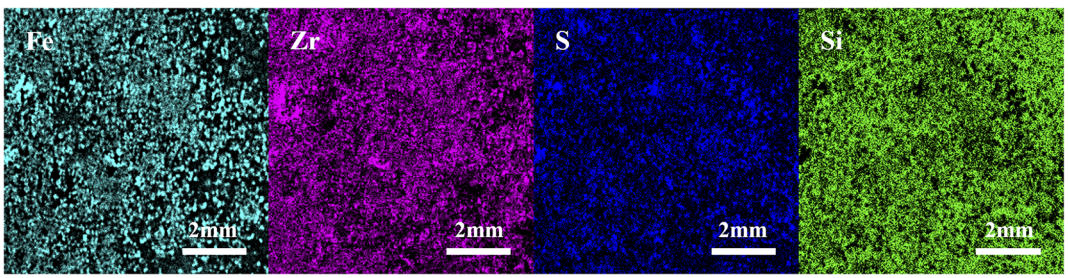

Fig. 3 The μ-XRF images of the $Fe_2(SO_4)_3$&$Zr(SO_4)_2$@diatomite catalyst.

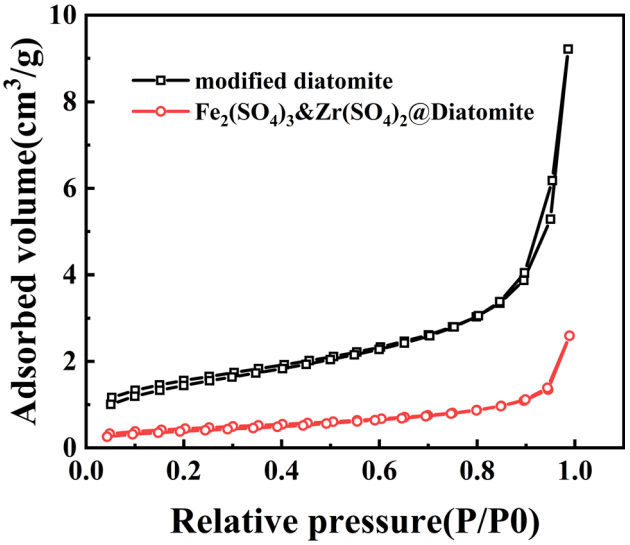

Fig. 5 The N_2 adsorption/desorption isotherms of modified diatomite and the $Fe_2(SO_4)_3$&$Zr(SO_4)_2$@diatomite catalyst.

to 1.54 $m^2\ g^{-1}$ after loading, which indicated the effective loading of $Fe_2(SO_4)_3$ and $Zr(SO_4)_2$. The pore size distribution curves of the modified diatomite and the catalyst are shown in Fig. 6. It was observed that the pore sizes of the samples before and after loading were all concentrated between 4 and 30 nm. This result indicated that the catalyst still retained obvious porosity. However, the pore volume of the catalyst (0.004 $cm^3\ g^{-1}$) was obviously lower than that of the modified diatomite (0.013 $cm^3\ g^{-1}$), which indicated that $Fe_2(SO_4)_3$ and $Zr(SO_4)_2$ were not only deposited on the surface but also on the pores.

3.1.6 TG. The thermal property of $Fe_2(SO_4)_3$&$Zr(SO_4)_2$@-diatomite catalyst was investigated. Fig. 7 shows the TG analysis results, and the first decrease in mass, observed from the start of the analysis up to about 200 °C may correspond to the amount of absorbed water. The rapid decrease in mass between

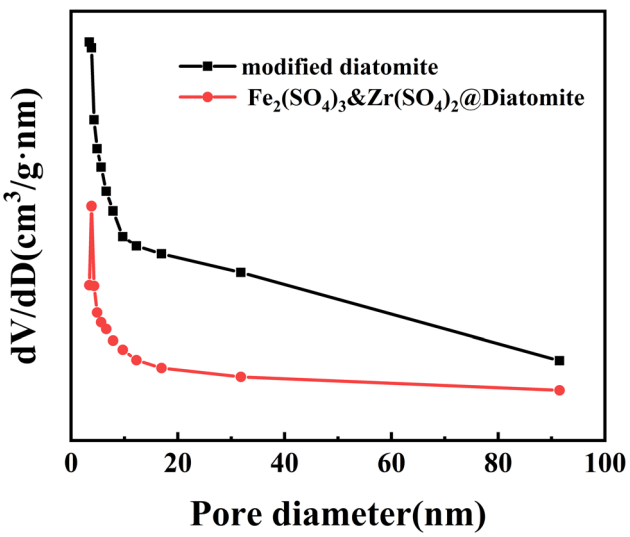

Fig. 6 Pore size distribution curves of modified diatomite and $Fe_2(SO_4)_3$&$Zr(SO_4)_2$@diatomite catalyst.

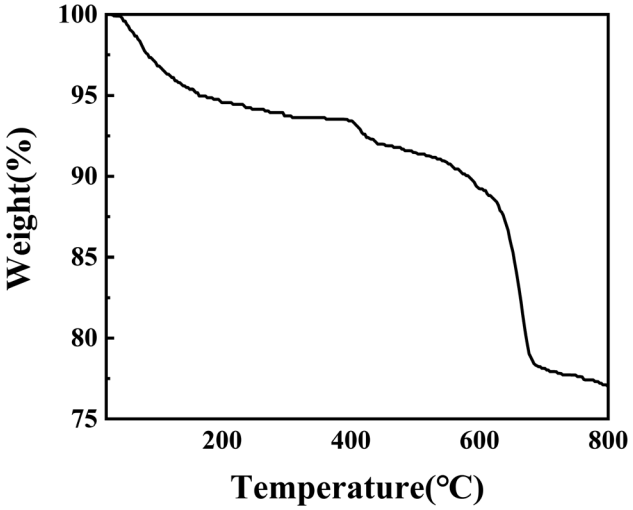

Fig. 7 The TG curve of $Fe_2(SO_4)_3$&$Zr(SO_4)_2$@diatomite catalyst.

610 °C and 702 °C was explained by the desulfurisation of $Fe_2(SO_4)_3$ and $Zr(SO_4)_2$. These results were consistent with those found in the literature.[36,79,80] Hence, the catalyst synthesised showed a good thermal property, which was beneficial to its stability.

3.2 Optimum conditions in the esterification process

The effects of the methanol/oil ratio, catalyst concentration, reaction temperature, and reaction time on the esterification rate were investigated using orthogonal experiments (see the ESI for the Experimental details†). The optimum conditions obtained were: methanol/oil ratio: 1.25 : 1, catalyst concentration: 10%, reaction temperature: 70 °C, and reaction time: 4 h.

3.3 Catalytic activity comparison

We also synthesised $Fe_2(SO_4)_3$@diatomite and $Zr(SO_4)_2$@-diatomite according to the method described in Section 2.2.2 for further investigation of the catalytic property of $Fe_2(SO_4)_3$&$Zr(SO_4)_2$@diatomite. The catalytic effects of the following catalysts: $Fe_2(SO_4)_3 \cdot xH_2O$, $Zr(SO_4)_2 \cdot 4H_2O$, $Fe_2(SO_4)_3$@-diatomite, $Zr(SO_4)_2$@diatomite and $Fe_2(SO_4)_3$&$Zr(SO_4)_2$@-diatomite in the esterification of waste fatty acids and methanol were compared using the method described in Section 2.2.4. Table 1 shows the results, and it was observed that the conversions of $Fe_2(SO_4)_3 \cdot xH_2O$, $Zr(SO_4)_2 \cdot 4H_2O$, $Fe_2(SO_4)_3$@-diatomite and $Zr(SO_4)_2$@diatomite were 94.40%, 97.75%, 95.22% and 98.56%, respectively, whereas that of $Fe_2(SO_4)_3$&-$Zr(SO_4)_2$@diatomite was 98.90% when the identical reaction parameters were adopted. It was quite clear that the composited $Fe_2(SO_4)_3$&$Zr(SO_4)_2$@diatomite showed a better catalytic performance than $Fe_2(SO_4)_3 \cdot xH_2O$, $Zr(SO_4)_2 \cdot 4H_2O$, $Fe_2(SO_4)_3$@diatomite and $Zr(SO_4)_2$@diatomite.

3.4 Reusability of the catalyst

Reusability is a pivotal property of solid catalysts and is closely tied to their affordability and potential applications. The

Table 1 Catalytic performances of $Fe_2(SO_4)_3$@diatomite, $Zr(SO_4)_2$@diatomite and $Fe_2(SO_4)_3$ and $Zr(SO_4)_2$@diatomite[a]

Trial number	Catalyst	Conversion (%)
1	$Fe_2(SO_4)_3 \cdot xH_2O$ (0.2 g)	94.40% ± 0.14
2	$Zr(SO_4)_2 \cdot 4H_2O$ (0.2 g)	97.75% ± 0.13
3	$Fe_2(SO_4)_3$@diatomite (0.5 g)	95.22% ± 0.19
4	$Zr(SO_4)_2$@diatomite (0.5 g)	98.56% ± 0.12
5	$Fe_2(SO_4)_3$&$Zr(SO_4)_2$@diatomite (0.5 g)	98.90% ± 0.16

[a] Waste fatty acids 5 g, methanol 6.25 g, reaction temperature 70 °C, reaction time 4 h.

reusability of $Fe_2(SO_4)_3$&$Zr(SO_4)_2$@diatomite was investigated by carrying out successive batch cycles using the same catalyst in the preparation of biodiesel using waste fatty acids, under the optimal parameters obtained from the orthogonal experiment (see ESI†). At the end of each batch run, the $Fe_2(SO_4)_3$&$Zr(SO_4)_2$@diatomite was recycled using simple filtration. The recycled catalyst was washed with methanol to remove the residual oils, and then dried in a vacuum oven at 40 °C, and then reused in the next esterification experiment. The experiments were carried out for four cycles and the outcomes are displayed in Fig. 8. This demonstrated that the conversion decreased slightly after three successive catalytic cycles, but it was still 91.56% after three cycles. Therefore, it was concluded that the $Fe_2(SO_4)_3$&$Zr(SO_4)_2$@diatomite catalyst was reusable, and had the potential to be applied as an efficient solid catalyst in biodiesel production. However, a significant decrease was observed after four cycles. The stability and water resistance of the diatomite supported $Fe_2(SO_4)_3$ and $Zr(SO_4)_2$ were significantly improved, but it might still dissolve slightly in water, a by-product of the esterification reaction. Considering the existence of the Fe–O–Si and Zr–O–Si bonds in the catalyst, which were demonstrated by the FTIR spectra, it was speculated that the diminishing of the catalytic activity may be mainly caused by the loss of SO_4^{2-}, which was soluble in water, rather than the loss of Zr^{4+} and Fe^{3+}.

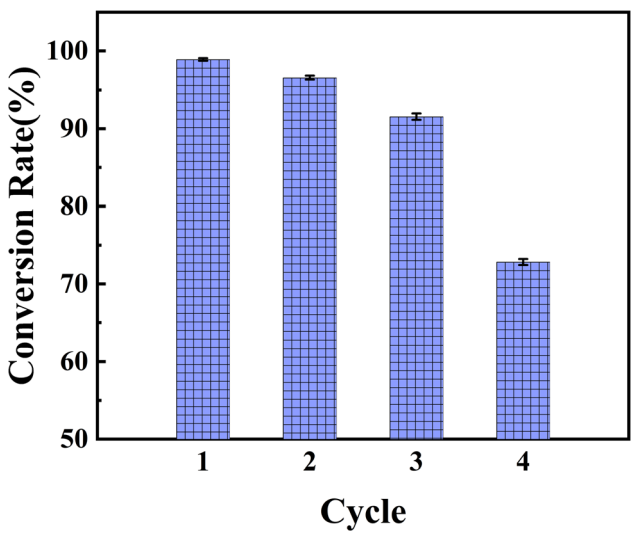

Fig. 8 Reusability of $Fe_2(SO_4)_3$&$Zr(SO_4)_2$@diatomite catalyst under optimal conditions.

3.5 Properties of biodiesel prepared from waste fatty acids

In order to collect enough samples to determine the properties of biodiesel, a larger experiment was carried out under optimal conditions (see Section 3.2) according to the method described in Section 2.2.4. During the industrial process, biodiesel prepared from waste oils usually required refining (vacuum distillation) to ensure its properties met those of the relevant standards. Hence, vacuum distillation (temperature: 250 °C, vacuum degree: 0.097 MPa) was performed before determining the properties of the biodiesel prepared from waste fatty acids. The acid value of refined biodiesel measured according to standard EN 14104 was 0.44 mg KOH per g, the density at 15 °C obtained by using a hydrometer according to standard EN ISO 3675 was 882 kg m^{-3}, and the flash point detected by using the Pensky–Martens closed cup method according to standard EN ISO 2719 was 179 °C. These properties met the requirements of European standard EN 14214: which states that the acid value should not exceed 0.5 mg KOH per g, density (15 °C) should be in the range of 860–900 kg m^{-3}, and the flash point should be higher than 101 °C.

4 Conclusions

We synthesised a $Fe_2(SO_4)_3$&$Zr(SO_4)_2$@diatomite catalyst by a simple impregnation and calcination process, and applied it in the esterification of waste fatty acids with methanol as a solid acid catalyst. The catalytic activity of the synthesised diatomite supported catalyst is superior to that of neat $Fe_2(SO_4)_3 \cdot xH_2O$ and neat $Zr(SO_4)_2 \cdot 4H_2O$ due to the loading of the active ingredient onto diatomite, which improves the dispersion and water-resistance of the active ingredient. Moreover, the catalytic activity of this catalyst is superior to that of $Fe_2(SO_4)_3$@diatomite and $Zr(SO_4)_2$@diatomite, benefiting from the synergistic effect of $Fe_2(SO_4)_3$ and $Zr(SO_4)_2$. The conversion of waste fatty acids catalysed by the $Fe_2(SO_4)_3$&$Zr(SO_4)_2$@diatomite reached 98.90% under optimal parameters (MeOH to oil ratio 1.25 : 1; catalyst concentration 10 wt%, reaction temperature 70 °C, reaction time 4 h). These optimal parameters obtained may be useful in the actual biodiesel production process.

The catalyst can also be recycled simply from reaction system *via* filtration, and then reapplied for multiple cycles without a noticeable decrease in catalytic activity, and the conversion remained at 91.56% after three cycles.

The catalyst in this work is simple to prepare, highly efficient and economical, which is beneficial for industrial applications. In addition, some reported diatomite-supported catalysts, such as diatomite-supported CaO/MgO,[54] diatomite-supported KOH[55] and diatomite-supported CaO,[56] cause saponification when the waste oils contain high amounts of fatty acids. The $Fe_2(SO_4)_3$&$Zr(SO_4)_2$@diatomite as an acid heterogeneous catalyst can catalyse the esterification and transesterification reactions simultaneously. Hence, it may be suited to the catalysis of biodiesel production from waste oils containing high amounts of fatty acids.

Author contributions

Weiqing Chen: conceptualisation, methodology, investigation, data curation and writing – original draft. Zhaoji Wu: visualisation. Ruoxue Peng and Wenjuan Wu: formal analysis. Xiaonan Li and Dan Cao: validation. Zhigang Zhang: conceptualisation, methodology, writing – review and editing, funding acquisition and supervision. Kui Niu: funding acquisition and supervision.

Conflicts of interest

There are no conflicts to declare.

Acknowledgements

This work was financially supported by a project for the Hebei Provincial Central Government Guides Local Science and Technology Development (Grant No. 206Z2801G).

References

1 S. K. R. Devasani, S. Vodnala, D. Singarapu and J. N. Nair, *Environ. Sci. Pollut. Res.*, 2021, **29**, 51083–51094.
2 P. S. Nigam and A. Singh, *Prog. Energy Combust. Sci.*, 2011, **37**, 52–68.
3 H. H. Mardhiah, H. C. Ong, H. H. Masjuki, S. Lim and H. V. Lee, *Renewable Sustainable Energy Rev.*, 2017, **67**, 1225–1236.
4 N. Pranyoto, Y. D. Susanti, I. J. Ondang, A. E. Angkawijaya, F. E. Soetaredjo, S. P. Santoso, M. Yuliana, S. Ismadji and S. B. Hartono, *Nanomaterials*, 2022, **12**, 245.
5 C. D. M. de Araújo, C. C. de Andrade, E. D. S. e Silva and F. A. Dupas, *Renewable Sustainable Energy Rev.*, 2013, **27**, 445–452.
6 B. A. Oni and D. Oluwatosin, *Renewable Energy*, 2020, **149**, 725–734.
7 Y. Ulusoy, *Environ. Sci. Pollut. Res.*, 2019, **27**, 500–509.
8 J. Chang, X. Guan, S. Pan, M. Jia, Y. Chen and H. Fan, *New J. Chem.*, 2018, **42**, 13074–13080.
9 P. Maheswari, M. B. Haider, M. Yusuf, J. J. Klemeš, A. Bokhari, M. Beg, A. Al-Othoman, R. Kumar and A. K. Jaiswal, *J. Cleaner Prod.*, 2022, **355**, 131588.
10 T. Tamoradi, A. R. Kiasat, H. Veisi, V. Nobakht and B. Karmakar, *New J. Chem.*, 2021, **45**, 21116–21124.
11 A. Pramanik and S. Bhar, *New J. Chem.*, 2021, **45**, 16355–16388.
12 M. Mohadesi, B. Aghel, M. Maleki and A. Ansari, *Renewable Energy*, 2019, **136**, 677–682.
13 M. Hamza, M. Ayoub, R. B. Shamsuddin, A. Mukhtar, S. Saqib, I. Zahid, M. Ameen, S. Ullah, A. G. Al-Sehemi and M. Ibrahim, *Environ. Technol. Innovation*, 2021, **21**, 101200.
14 J. Gupta, M. Agarwal and A. K. Dalai, *J. Ind. Eng. Chem.*, 2020, **88**, 58–77.
15 I. Raheem, M. N. B. Mohiddin, Y. H. Tan, J. Kansedo, N. M. Mubarak, M. O. Abdullah and M. L. Ibrahim, *J. Ind. Eng. Chem.*, 2020, **91**, 54–68.
16 M. O. Faruque, S. A. Razzak and M. M. Hossain, *Catalysts*, 2020, **10**, 1025.
17 B. Changmai, R. Rano, C. Vanlalveni and L. Rokhum, *Fuel*, 2021, **286**, 119447.
18 A. Wang, P. Sudarsanam, Y. Xu, H. Zhang, H. Li and S. Yang, *Green Chem.*, 2020, **22**, 2977–3012.
19 L. F. Man, T. L. Kwong, W. T. Wong and K. F. Yung, *Nanomaterials*, 2021, **11**, 2690.
20 M. Dionicio-Navarrete, C. D. Arrieta-Gonzalez, A. Quinto-Hernandez, M. Casales-Diaz, J. Zuñiga-Diaz, J. Porcayo-Calderon and L. Martinez-Gomez, *Nanomaterials*, 2019, **9**, 1545.
21 F. Núñez, L. F. Chen, J. A. Wang, S. O. Flores, J. Salmones, U. Arellano, L. E. Noreña and F. Tzompantzi, *Catalysts*, 2022, **12**, 900.
22 C. C. Huang, S. H. Ho, J. S. Chang and P. J. Gao, *New J. Chem.*, 2020, **44**, 13669–13684.
23 B. Lowe, J. Gardy and A. Hassanpour, *Catalysts*, 2022, **12**, 223.
24 Y. Li, X. D. Zhang, L. Sun, J. Zhang and H. P. Xu, *Appl. Energy*, 2010, **87**, 156–159.
25 D. Guan, M. Fan, J. Wang, Y. Zhang, Q. Liu and X. Jing, *Mater. Chem. Phys.*, 2010, **122**, 278–283.
26 Y. Feng, A. Zhang, J. Li and B. He, *Bioresour. Technol.*, 2011, **102**, 3607–3609.
27 J. Fu, L. Chen, P. Lv, L. Yang and Z. Yuan, *Fuel*, 2015, **154**, 1–8.
28 N. Siddique, M. Suzue, M. Kato, K. Hiromori and N. Shibasaki-Kitakawa, *Fuel*, 2021, **289**, 119884.
29 M. A. Hanif, S. Nisar and U. Rashid, *Catal. Rev.*, 2017, **59**, 165–188.
30 F. Esmi, V. B. Borugadda and A. K. Dalai, *Catal. Today*, 2022, **404**, 19–34.
31 W. Xie, C. Gao and J. Li, *Renewable Energy*, 2021, **168**, 927–937.
32 R. Leesing, S. Siwina and K. Fiala, *Renewable Energy*, 2021, **171**, 647–657.
33 R. R. C. Bastos, A. P. Luz Corrêa, P. T. S. Luz, G. N. Rocha Filho, J. R. Zamian and L. R. V. Conceição, *Energy Convers. Manage.*, 2020, **205**, 112457.
34 M. A. Farabi, M. L. Ibrahim, U. Rashid and Y. H. Taufiq-Yap, *Energy Convers. Manage.*, 2019, **181**, 562–570.
35 P. Yu, C. Chen, G. Li, Z. Wang and X. Li, *Catalysts*, 2020, **10**, 384.
36 M. I. Senoymak Tarakcı and O. Ilgen, *Chem. Eng. Technol.*, 2018, **41**, 845–852.
37 R. Nakamura, K. Komura and Y. Sugi, *Catal. Commun.*, 2008, **9**, 511–515.
38 F. P. Martins, F. A. Rodrigues and M. J. Silva, *Energies*, 2018, **11**, 1263.
39 Y. Pan, Y. Liu and C. Liu, *J. Power Sources*, 2015, **285**, 169–177.
40 U. T. Uthappa, V. Brahmkhatri, G. Sriram, H. Y. Jung, J. Yu, N. Kurkuri, T. M. Aminabhavi, T. Altalhi, G. M. Neelgund and M. D. Kurkuri, *J. Controlled Release*, 2018, **281**, 70–83.
41 X. W. Sun, Y. X. Zhang and D. Losic, *J. Mater. Chem. A*, 2017, **5**, 8847–8859.

42 P. A. Zong, D. Makino, W. Pan, S. Yin, C. Sun, P. Zhang, C. Wan and K. Koumoto, *Mater. Des.*, 2018, **154**, 246–253.
43 C. Li, M. Wang, Z. Chen and J. Chen, *J. Energy Storage*, 2021, **34**, 102171.
44 F. Jiang, Z. Ge, X. Ling, D. Cang, L. Zhang and Y. Ding, *Renewable Energy*, 2021, **179**, 327–338.
45 D. B. Jiang, X. Liu, Y. Yuan, L. Feng, J. Ji, J. Wang, D. Losic, H. C. Yao and Y. Z. Zhang, *Chem. Eng. J.*, 2020, **383**, 123156.
46 G. Sriram, U. T. Uthappa, D. Losic, M. Kigga, H. Y. Jung and M. D. Kurkuri, *Appl. Sci.*, 2020, **10**, 2285.
47 Y. Tan, S. Zheng, Y. Di, C. Li, R. Bian and Z. Sun, *J. Mater. Sci. Technol.*, 2021, **95**, 57–69.
48 L. Bengotni, B. Trari, B. Lebeau, L. Michelin, L. Josien, A. Benguedach and R. Hamacha, *New J. Chem.*, 2021, **45**, 13463–13474.
49 U. T. Uthappa, G. Sriram, O. R. Arvind, S. Kumar, H. Y. Jung, G. M. Neelgund, D. Losic and M. D. Kurkuri, *Appl. Surf. Sci.*, 2020, **528**, 146974.
50 I. Ruggiero, M. Terracciano, N. M. Martucci, L. De Stefano, N. Migliaccio, R. Tatè, I. Rendina, P. Arcari, A. Lamberti and I. Rea, *Nanoscale Res. Lett.*, 2014, **9**, 1–7.
51 M. Terracciano, M. A. Shahbazi, A. Correia, I. Rea, A. Lamberti, L. De Stefano and H. A. Santos, *Nanoscale*, 2015, **7**, 20063–20074.
52 N. Ezzatahmadi, T. Bao, H. Liu, G. J. Millar, G. A. Ayoko, J. Zhu, R. Zhu, X. Liang, H. He and Y. Xi, *RSC Adv.*, 2018, **8**, 7687–7696.
53 G. Zhang, A. Peyravi, Z. Hashisho, Z. Sun, Y. Liu, S. Zheng and L. Zhong, *Catal. Sci. Technol.*, 2020, **10**, 2378–2388.
54 A. M. Rabie, M. Shaban, M. R. Abukhadra, R. Hosny, S. A. Ahmed and N. A. Negm, *J. Mol. Liq.*, 2019, **279**, 224–231.
55 E. Modiba, C. Enweremadu and H. Rutto, *Chin. J. Chem. Eng.*, 2015, **23**, 281–289.
56 R. Shan, C. Zhao, H. Yuan, S. Wang and Y. Wang, *Energy Convers. Manage.*, 2017, **138**, 547–555.
57 S. M. Pavlović, D. M. Marinković, M. D. Kostić, I. M. Janković-Častvan, L. V. Mojović, M. V. Stanković and V. B. Veljković, *Fuel*, 2020, **267**, 117171.
58 L. Du, S. Ding, Z. Li, E. Lv, J. Lu and J. Ding, *Energy Convers. Manage.*, 2018, **173**, 728–734.
59 J. K. Karo, H. Husin, F. Nasution, F. T. Yani, S. Maliki, D. D. Prayuda and F. Hasfita, *IOP Conf. Ser.: Mater. Sci. Eng.*, 2020, **980**, 012058.
60 A. S. Yusuff, J. O. Owolabi and S. Afr, *J. Chem. Eng.*, 2019, **30**, 42–49.
61 Z. Helwani, I. Zahrina, S. Z. Amraini, R. I. Sianturi, G. M. Idroes and R. Idroes, *IOP Conf. Ser.: Mater. Sci. Eng.*, 2021, **1087**, 012053.
62 L. J. Konwar, J. Boro and D. Deka, *Energy Sources, Part A*, 2018, **40**, 601–607.
63 *The price of diatomite and activated carbon online*, **https://b2b.baidu.com**, accessed January 2023.
64 *The price of alumina and zeolite online*, **https://jsx888.51sole.com/companynewsdetail_134118715.html**, accessed January 2023.
65 L. Ma, Y. Han, K. Sun, J. Lu and J. Ding, *Energy Convers. Manage.*, 2015, **98**, 46–53.
66 M. Guo, W. Jiang, C. Chen, S. Qu, J. Lu, W. Yi and J. Ding, *Energy Convers. Manage.*, 2021, **229**, 113745.
67 S. Yusan, K. Korzhynbayeva, S. Aytas, S. Tazhibayeva and K. Musabekov, *J. Alloys Compd.*, 2014, **608**, 8–13.
68 J. C. Juan, J. Zhang and M. A. Yarmo, *Appl. Catal., A*, 2008, **347**, 133–141.
69 L. Chen, J. Xu and J. Hu, *J. Radioanal. Nucl. Chem.*, 2013, **297**, 97–105.
70 D. L. Zhao, S. J. Feng, C. L. Chen, S. H. Chen, D. Xu and X. K. Wang, *Appl. Clay Sci.*, 2008, **41**, 17–23.
71 G. Yao, J. Lei, X. Zhang, Z. Sun, S. Zheng and S. Komarneni, *Mater. Res. Bull.*, 2018, **107**, 132–138.
72 S. G. Jeong, J. Jeon, J. H. Lee and S. Kim, *Int. J. Heat Mass Transfer*, 2013, **62**, 711–717.
73 I. Cacciotti, M. Rinaldi, J. Fabbrizi and F. Nanni, *J. Mater. Res. Technol.*, 2019, **8**, 1737–1745.
74 L. Jiang, L. Liu, S. Xiao and J. Chen, *Chem. Eng. J.*, 2016, **284**, 609–619.
75 H. Hamad, M. A. El-Latif, A. E. H. Kashyout, W. Sadik and M. Feteha, *New J. Chem.*, 2015, **39**, 3116–3128.
76 S. Kongwudthiti, P. Praserthdam, W. Tanakulrungsank and M. Inoue, *J. Mater. Process. Technol.*, 2003, **136**, 186–189.
77 P. Salas, J. A. Wang, H. Armendariz, C. Angeles-Chavez and L. F. Chen, *Mater. Chem. Phys.*, 2009, **114**, 139–144.
78 Y. Xia, F. Li, Y. Jiang, M. Xia, B. Xue and Y. Li, *Appl. Surf. Sci.*, 2014, **303**, 290–296.
79 Q. Liu, C. Q. Wang, J. Tan, Z. L. Yin, Q. Y. Chen, Z. Liao, P. M. Zhang and Y. Liu, *J. Cent. South Univ.*, 2015, **22**, 1256–1263.
80 S. M. Pérez-Moreno, M. J. Gázquez, A. G. Barneto and J. P. Bolívar, *Thermochim. Acta*, 2013, **552**, 114–122.